

Locations of Accretion Shocks around Galaxy Clusters and the ICM properties: insights from Self-Similar Spherical Collapse with arbitrary mass accretion rates

Xun Shi [★]

Max-Planck-Institut für Astrophysik, Karl-Schwarzschild-Straße 1, D-85740 Garching bei München, Germany

29 June 2016

ABSTRACT

Accretion shocks around galaxy clusters mark the position where the infalling diffuse gas is significantly slowed down, heated up, and becomes a part of the intracluster medium (ICM). They play an important role in setting the ICM properties. Hydrodynamical simulations have found an intriguing result that the radial position of this accretion shock tracks closely the position of the ‘splashback radius’ of the dark matter, despite the very different physical processes that gas and dark matter experience. Using the self-similar spherical collapse model for dark matter and gas, we find that an alignment between the two radii happens only for a gas with an adiabatic index of $\gamma \approx 5/3$ and for clusters with moderate mass accretion rates. In addition, we find that some observed ICM properties, such as the entropy slope and the effective polytropic index lying around $\sim 1.1 - 1.2$, are captured by the self-similar spherical collapse model, and are insensitive to the mass accretion history.

Key words: galaxies: clusters: general – galaxies: clusters: intracluster medium – cosmology: theory – methods: analytical

1 INTRODUCTION

When diffuse gas is accreted on to a galaxy cluster, it inevitably goes through an accretion shock in the cluster outskirts. X-ray and the Sunyaev-Zel’dovich effect observations now start to reach the sensitivities required to probe the outer regions of galaxy clusters (e.g. Planck Collaboration XL 2015, see also Reiprich et al. 2013 for a review), and we may expect a direct detection of the accretion shock in the near future. This motivates our studying where we expect to find the accretion shock, as well as the properties of the intracluster gas in the bulk of the cluster volume.

In hydrodynamical simulations, there exists a complex network of accretion shocks outside the virial radius of a galaxy cluster due to the inhomogeneous distribution of matter there (Kang et al. 2007; Vazza et al. 2011; Planelles & Quilis 2013). Nevertheless, the peak of the entropy profile provides us with a unique practical definition of the radial position of the accretion shock (Lau et al. 2015). This definition of the shock radius is convenient particularly because it can also be inferred from observations. Using this definition, Lau et al. (2015) found that the shock radius is slightly larger than, but tracks closely the splashback radius of the dark matter (Diemer & Kravtsov 2014; Adhikari, Dalal & Chamberlain 2014; More, Diemer & Kravtsov 2015) despite of the very different underlying physics. The two radii align with each other to an extent

that the resulting ratio of gas density and dark matter density stays close to the cosmic mean value over a large radial range in the cluster outskirts (Fig. 9 of Lau et al. 2015), although the density jumps associated with the shock and splashback radii may easily cause a large deviation. Moreover, both the accretion shock radius and the splashback radius scale well with r_{200m} – the radius within which the averaged density is 200 times the *mean* density of the universe, rather than the more commonly used r_{200c} (for which the reference density is the *critical* density of the universe) which is better for scaling the cluster inner profiles (Lau et al. 2015).

To explore the origin of these curious behaviors, one needs to study the growth of galaxy clusters in an expanding universe by accreting matter around them. The self-similar spherical collapse model (Bertschinger 1985) offers us the simplest analytical framework for doing this. With the self-similarity ansatz alone, the self-similar spherical collapse model allows us to rigorously and consistently derive the self-similarity profiles of the collapsed regions, e.g. galaxy clusters. This distinguishes it from the other smooth accretion models (Tozzi & Norman 2001; Voit et al. 2003) which need further assumptions about the internal structure of the galaxy cluster.

A somewhat overlooked fact is that the self-similar spherical collapse solutions given in Bertschinger (1985) have already captured an alignment between the accretion shock radius and the splashback radius, as well as some observed ICM properties such as the slope of the entropy profile and the effective equation of state of

[★] E-mail: xun@mpa-garching.mpg.de

the intracluster gas. However, Bertschinger (1985) studied only one particular shape of the initial density peak which corresponds to a particular mass accretion rate of a galaxy cluster. Since the mass accretion rate is known to play an important role in determining the locations of the accretion shock, the splashback radius, as well as the ICM profiles (e.g. Diemer & Kravtsov 2014; Adhikari, Dalal & Chamberlain 2014; Lau et al. 2015), it is hard to tell whether the features captured by the Bertschinger (1985) model hold at an arbitrary mass accretion rate, or are just coincidences occurring at that particular mass accretion rate.

Inspired by the success of the Bertschinger model and motivated by this shortcoming, we explore the properties of self-similar spherical collapse solutions systematically by extending Bertschinger's scheme to various mass accretion rates. We also consider the effect of a different inner mass profile due to dynamical relaxation, and the dynamical effect of a finite baryon content (Bertschinger 1985 considered only the case of a negligible baryon content, i.e. $\Omega_b \ll \Omega_m$).

We will focus on the following physical questions:

- What determines the radial position of the accretion shock? Why does it track closely the splashback radius of the dark matter?
- What sets the entropy slope and the effective equation of state of the intracluster gas?
- The accretion shock slows down the gas compared to the dark matter during their accretion on to a galaxy cluster - how does this affect the gas mass fraction inside the cluster?

We describe the self-similar spherical collapse and its various representations in Sect. 2. In Sect. 3 we explore the physical origin of the accretion shock location, why it aligns well with the dark matter splashback radius, and how it is affected by a modification of the inner mass profile and a finite baryon fraction. In Sect. 4 we study the ICM properties including the entropy profile, the effective equation of state of the intracluster gas, and the gas mass fraction. We discuss how these results would be affected by the deviation from smooth accretion and the existence of dark energy in Sect. 5, and conclude in Sect. 6.

2 SELF-SIMILAR SPHERICAL COLLAPSE AND ITS VARIOUS REPRESENTATIONS

We study a secondary infall of a mass shell on to an initial overdense region that would grow to a halo of the size of a galaxy cluster. The profile of the initial mass excess we consider is of a power-law shape, $\delta m_i/m_i \propto m_i^{-1/s}$. In an Einstein de-Sitter (EdS) universe, this initial overdensity profile implies a power-law mass growth $m \propto a^s$ of the halo (e.g. Fillmore & Goldreich 1984), with a being the cosmic scale factor. The sizes of these overdense regions are much smaller than that of the horizon. These, together with a scale-free EdS cosmological background, ensure that the growth of the halos is self-similar, as were the cases considered by Fillmore & Goldreich (1984) and Bertschinger (1985).

Self-similarity suggests that the trajectory of a single shell of matter (matter at a certain Lagrangian radius) describes at the same time the positions of all the shells in one snapshot, i.e. the profile of the matter distribution. In fact, the trajectories and profiles couple in the dynamical equations, and thus need to be solved together. The solutions can also be presented in both a ‘trajectory view’ and a ‘profile view’, which complement each other. In the following we present both views of the self-similar infall process.

We consider the self-similar infall trajectories of cold dark

matter and gas. A spherical shell of gas obeys the equation of motion

$$\frac{d^2 r}{dt^2} = -\frac{Gm}{r^2} - \frac{1}{\rho} \frac{\partial p}{\partial r}, \quad (1)$$

while for dark matter there is no pressure force (the second term on the r.h.s.). The mass m represents the total mass of dark matter and gas. We consider an initial gas mass fraction equal to a cosmic mean value Ω_b/Ω_m . At first we consider $\Omega_b = 0$, i.e. assume that the mass is fully dominated by the dark matter, and study the effect of a finite baryon content Ω_b in Sect. 3.3.

As the typical temperature of the intergalactic diffuse gas is several orders of magnitude lower than that of the intracluster gas, we neglect the temperature and pressure in the gas before it gets shocked upon entering the pre-existing halo. With this cold-accretion assumption, gas and dark matter are dynamically indistinguishable before the accretion shock. The enclosed total mass stays at its initial value m_i during their initial expansion with the universe until the common trajectory turns around at a time t^* and radius r^* due to the excess mass contained in m_i . After the turn-around, the gas experiences an accretion shock at some radius, which slows down and separates it dynamically from the collisionless dark matter.

Bertschinger (1985) realised that, thanks to self-similarity, the total mass profile must have a universal shape when normalised to the values at the current turn-around radius r_{ta}^1 . The same holds true for the individual gas and dark matter mass and density profiles as well as for the velocity and thermodynamical profiles of the gas. We define the nondimensional profiles of gas velocity V , density D , pressure P , and the total mass profile M as

$$\begin{aligned} v &= \frac{r_{ta}}{t} V(\lambda), \\ \rho &= \rho_H D(\lambda), \\ p &= \rho_H \left(\frac{r_{ta}}{t} \right)^2 P(\lambda), \\ m &= \frac{4\pi\rho_H}{3} r_{ta}^3 M(\lambda), \end{aligned} \quad (2)$$

with $\lambda = r/r_{ta}$ and ρ_H being the mean matter density in the universe, $\rho_H = 1/(6\pi G t^2)$. The equation of motion Eq. (1) can then be written in a form that has no explicit time dependence

$$\frac{d^2 \lambda}{d\xi^2} + (2\delta - 1) \frac{d\lambda}{d\xi} + \delta(\delta - 1)\lambda = -\frac{2}{9} \frac{M(\lambda)}{\lambda^2} - \frac{P'}{D}, \quad (3)$$

where the prime denotes taking derivative with respect to λ , and $\xi = \ln(t/t^*)$ is the new time variable. We have extended Bertschinger's original equation to an arbitrary mass growth rate s . Here, $\delta = 2(1 + s/3)/3$ bears the meaning of the time-dependence of the current turn-around radius, i.e. $r_{ta} \propto t^\delta$. This time-dependence of r_{ta} gives rise to the additional $d\lambda/d\xi$ and λ terms on the l.h.s. of Eq. (3). A natural choice of the initial condition for Eq. (3) is $\lambda = 1$ and $d\lambda/d\xi = \delta$ at turn-around, i.e. at $\xi = 0$. To help visualising how different forms of the dynamical equations match with each other, we summarise the expressions for the radial position, velocity and acceleration in terms of different variables in Table. 1.

Since dark matter is collisionless, a dark matter shell falls all

¹ We distinguish the quantities at the turn-around radius *of the shell* which we indicate using superscript ‘*’, to the quantities at the ‘current turn-around radius’ (the turn-around radius *at the time of observation*, i.e. $t^* = t^{obs}$) which we indicate with subscript ‘ta’.

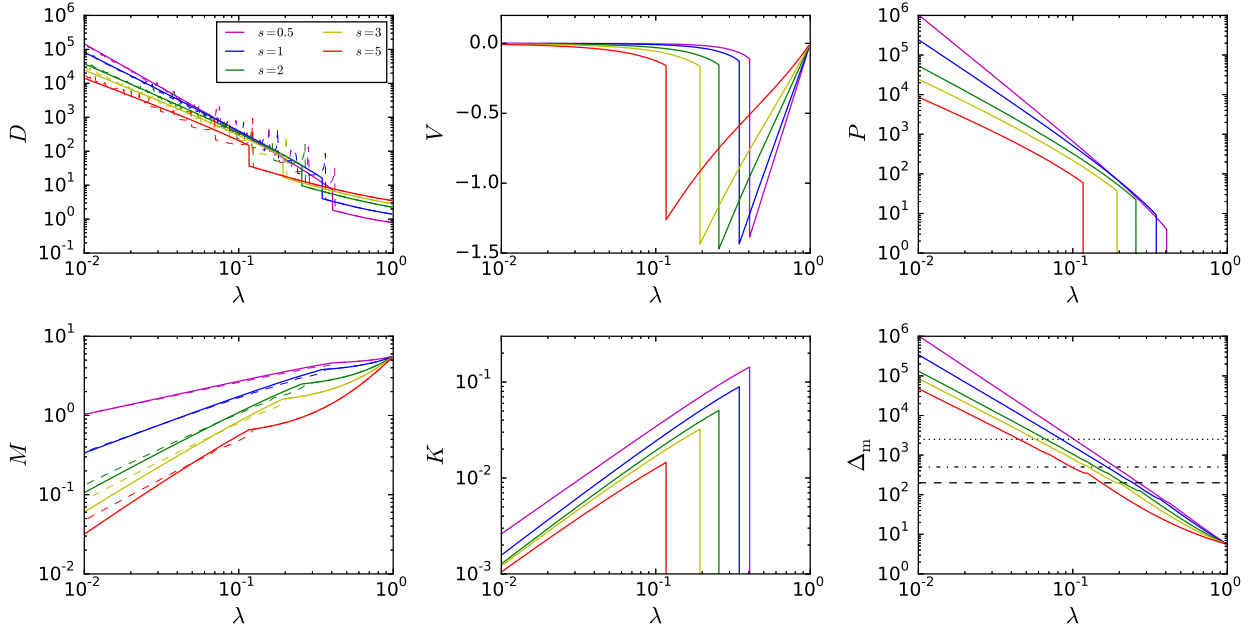


Figure 1. Radial profiles of the nondimensional gas density (upper left), velocity (upper middle), pressure (upper right), mass (lower left), entropy (lower middle), and averaged overdensity (lower right) in the self-similar spherical collapse model. Different colors indicate different mass accretion rates. In the left panels, the density and mass profiles of dark matter are plotted as the color dashed lines for comparison. The numerical values of the dark matter density at the caustics are artificially reduced for the clarity of the general profile shape. In the lower right panel, averaged overdensity of 200, 500, and 2500 are marked as the dashed, dash-dotted, and dotted lines to show the corresponding positions of commonly used radii r_{200} , r_{500} and r_{2500} . The default value of $\gamma = 5/3$ is taken for the adiabatic index of the gas.

Table 1. Dimensionless radial position, velocity and acceleration expressed with different variables.

variables	r, t	$\lambda = r/r_{\text{ta}}, \xi = \ln(t/t^*)$	$\lambda_F = r/r^*, \tau = t/t^*$	$V = vt/r_{\text{ta}}, \lambda = r/r_{\text{ta}}$
Radial position	$\frac{1}{r_{\text{ta}}(t)} r$	λ	$\tau^{-\delta} \lambda_F$	λ
Velocity	$\frac{t}{r_{\text{ta}}(t)} \frac{dr}{dt}$	$\frac{d\lambda}{d\xi} + \delta\lambda$	$\tau^{1-\delta} \frac{d\lambda_F}{d\tau}$	V
Acceleration	$\frac{r^2}{r_{\text{ta}}(t)} \frac{d^2 r}{dt^2}$	$\frac{d^2 \lambda}{d\xi^2} + (2\delta - 1) \frac{d\lambda}{d\xi} + \delta(\delta - 1)\lambda$	$\tau^{2-\delta} \frac{d^2 \lambda_F}{d\tau^2}$	$(V - \delta\lambda)V' + (\delta - 1)V$

the way to the center of the cluster and then continues to move outward until reaching the so-called splashback radius λ_{sp} , and turns around again. The dark matter mass at $\lambda < \lambda_{\text{sp}}$ is then contributed by multiple dark matter streams accreted at different times.

Deriving the dark matter mass profile requires solving the pressure-less form of the equation of motion Eq. (3) iteratively together with

$$M(\lambda) = M_{\text{ta}} \sum_i (-1)^{i-1} \exp[-(2s/3)\xi_i], \quad (4)$$

where ξ_i is the value of ξ at the i th point with $\lambda = \lambda(\xi)$ (Bertschinger 1983, 1985). The alternating signs are related to adding/subtracting the contribution from dark matter streams moving inward/outward at radius λ . The $2s/3$ factor in the exponent is related to the fact that the mass enclosed in a certain radius λ grows with time as $m(\lambda r_{\text{ta}}, t) \propto t^{2s/3}$. The $M_{\text{ta}} = (3\pi/4)^2 \approx 5.55$ prefactor is the overdensity at turn-around (e.g. Lacey & Cole 1993).

As for gas, we seek the solution of a single self-similar accretion shock that stays at a fixed λ_{sh} (Bertschinger 1985). In the Eulerian coordinate this corresponds to an outward propagating shock front with velocity $v_{\text{sh}} = \delta\lambda_{\text{sh}} r_{\text{ta}}/t$. For $\lambda > \lambda_{\text{sh}}$, i.e. before the shock passage, the gas velocity is derivable from the trajectory as $V = d\lambda/d\xi + \delta\lambda$, and its mass is $M_{\text{gas}}(\lambda) = M_{\text{ta}} \exp[-(2s/3)\xi_1]$.

After going through the accretion shock, the gas obtains a non-negligible pressure whose dynamical effect needs to be accounted for in the fluid equations

$$\begin{aligned} \frac{d\rho}{dt} &= -\frac{\rho}{r^2} \frac{\partial}{\partial r} (r^2 v), \\ \frac{dv}{dt} &= -\frac{Gm}{r^2} - \frac{1}{\rho} \frac{\partial p}{\partial r}, \\ \frac{d}{dt} (p\rho^{-\gamma}) &= 0, \\ \frac{\partial m_{\text{gas}}}{\partial r} &= 4\pi r^2 \rho. \end{aligned} \quad (5)$$

We have assumed that the gas is adiabatic with an equation of state γ . As a default we consider $\gamma = 5/3$, which is the value for monoatomic ideal gas. The nondimensional forms of these continuity,

Euler, adiabatic and mass equations are

$$\begin{aligned}
 [V - \delta\lambda] D' + DV' + \frac{2DV}{\lambda} - 2D &= 0, \\
 [V - \delta\lambda] V' + (\delta - 1)V &= -\frac{2}{9} \frac{M}{\lambda^2} - \frac{P'}{D}, \\
 [V - \delta\lambda] \left(\frac{P'}{P} - \gamma \frac{D'}{D} \right) &= -2(\gamma - 1) - 2(\delta - 1), \\
 M'_{\text{gas}} &= 3\lambda^2 D.
 \end{aligned} \tag{6}$$

They are solved with the outer boundary conditions at the accretion shock given by the shock jump conditions

$$\begin{aligned}
 V_2 &= \frac{\gamma - 1}{\gamma + 1} [V_1 - \delta\lambda_{\text{sh}}] + \delta\lambda_{\text{sh}}, \\
 D_2 &= \frac{\gamma + 1}{\gamma - 1} D_1, \\
 P_2 &= \frac{2}{\gamma + 1} D_1 [V_1 - \delta\lambda_{\text{sh}}]^2, \\
 M_2 &= M_1.
 \end{aligned} \tag{7}$$

The pre-shock velocity V_1 and density D_1 are given by the pre-shock gas velocity and mass profiles once the shock radius λ_{sh} is known. The shock radius is in turn determined by requiring the solutions of Eq. (6) to satisfy the inner boundary conditions $V(0) = 0$ and $M_{\text{gas}}(0) = 0$.

The resulting gas profiles are shown in Fig. 1 for various mass accretion rates $s = 0.5, 1, 2, 3$ and 5 . The nondimensional profiles of the gas density (upper left), velocity (upper middle), pressure (upper right), mass (lower left), entropy (lower middle), and averaged overdensity (lower right) all depend on the accretion rate s . In particular, the radial position of the accretion shock significantly decreases with an increasing accretion rate. The shapes of the profiles, on the other hand, show some regularity not sensitive to the accretion rate. For instance, the slope of the entropy profile remains unchanged with s , and the slopes of the density, pressure and mass profiles within the accretion shock saturate to a certain value at high accretion rates. We will discuss these behaviors in more detail in Sects. 3 and 4.

We also present the ‘trajectory view’ of the self-similarity solutions in Figs. 2 and 3, where the trajectories of dark matter and gas are normalised to the current turn-around radius r_{ta} and the turn-around radius of the shell r^* , respectively. From Fig. 2 one can clearly read out the splashback radius for the dark matter (the first peaks of the dashed lines after turn-around) and the accretion shock radius for the gas (where the solid lines start to deviate from the dashed lines). Both the splashback radius and the shock radius decrease from the turn-around radius with an increasing mass accretion rate s . These two radii follow each other closely for any accretion rate (indicated by the color of the lines). It is remarkable that this behavior, which was discovered previously in adiabatic hydrodynamical simulations for galaxy clusters (Lau et al. 2015), is already captured by the self-similarity solutions. This allows us to explore the origin of this alignment using a simple analytical framework, which we will do in Sect. 3.

When normalized to the current turn-around radius, the trajectories of both dark matter and gas reduce in amplitude with time (Fig. 2) due to the expansion of the current turn-around radius as the universe expands. In the Eulerian coordinate, however, the amplitudes of these trajectories do not necessarily shrink with time. Fig. 3 presents the trajectories normalized to their own turn-around radius r^* and time t^* by plotting $\lambda_F = r/r^*$ against $\tau = t/t^* = \exp(\xi)$ (Fillmore & Goldreich 1984). Over a long time scale, the am-

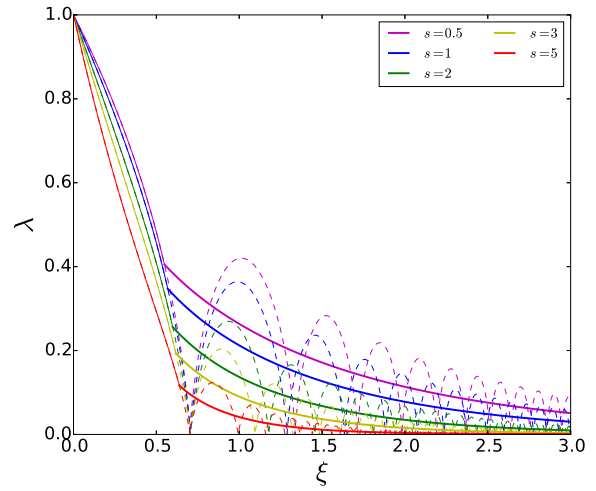


Figure 2. Trajectories of self-similar spherical infall of dark matter (dashed lines) and gas (solid lines) starting from turn-around. Infall trajectories with various mass accretion rates s are shown as the lines of different colors. The radii of the accreted shells are normalised to the current turn-around radius, i.e. $\lambda = r/r_{\text{ta}}$, and are plotted against the logarithmic time $\xi = \ln(t/t^*)$.

plitudes of the oscillating trajectories for dark matter continue to shrink due to the increase of mass within an Eulerian radius when $s > 3/2$ (Fillmore & Goldreich 1984), while remains constant when $s \leq 3/2$ (upper panel). The gas, on the other hand, always settles at a finite Eulerian radius within its shock radius (lower panel).

3 RADIAL POSITION OF THE ACCRETION SHOCK

3.1 Physical origin

We show the dependencies of the accretion shock position on the adiabatic index γ and the accretion rate s in Fig. 4. The accretion shock position λ_{sh} is larger for a higher accretion rate, and for a more stiff gas with a higher γ value.

What determines the radial position of the accretion shock? Strictly speaking, the radial position of the accretion shock λ_{sh} in the self-similar solutions is derived as an eigenvalue of the fluid equations by requiring them to satisfy the inner boundary conditions at $r = 0$. To gain physical insights, however, it is better to take the point of view of the infalling gas, in which the position where it will get shocked is specified by the shock jump conditions Eq. (7).

The shock jump conditions express the continuity of mass, momentum and enthalpy across the shock front. Given the properties of shock-bounded matter inside the halo, the accretion shock must occur at a position where the properties of the inflowing matter allow these continuities. Here, we use the simple framework of self-similar spherical collapse model to give approximations for both the pre-shock flow and the post-shock halo gas, and show that combining the two indeed sets the location of the accretion shock.

The infall velocity of the pre-shock flow relates to the shock position λ_{sh} through the conservation of the sum of kinetic and gravitational energy of the infalling gas. Namely, the kinetic energy at the position of the accretion shock should equal the difference of the gravitational energies at the accretion shock and the turn-around

Table 2. Tabular form of Fig. 4. Positions of the accretion shock for gas, $\lambda_{\text{sh}} = r_{\text{sh}}/r_{\text{ta}}$, with different equations of state γ (columns 2-6) and the splashback position, λ_{sp} , of the collisionless matter (column 7) for various accretion rates s .

	$\gamma = 3$	$\gamma = 2$	$\gamma = 5/3$	$\gamma = 3/2$	$\gamma = 4/3$	Collisionless, splashback
$s = 0.5$	0.650	0.501	0.405	0.329	0.216	0.420
$s = 1$	0.590	0.437	0.347	0.279	0.189	0.364
$s = 2$	0.482	0.332	0.256	0.202	0.136	0.270
$s = 3$	0.394	0.256	0.193	0.150	0.100	0.204
$s = 5$	0.265	0.159	0.117	0.089	0.059	0.123

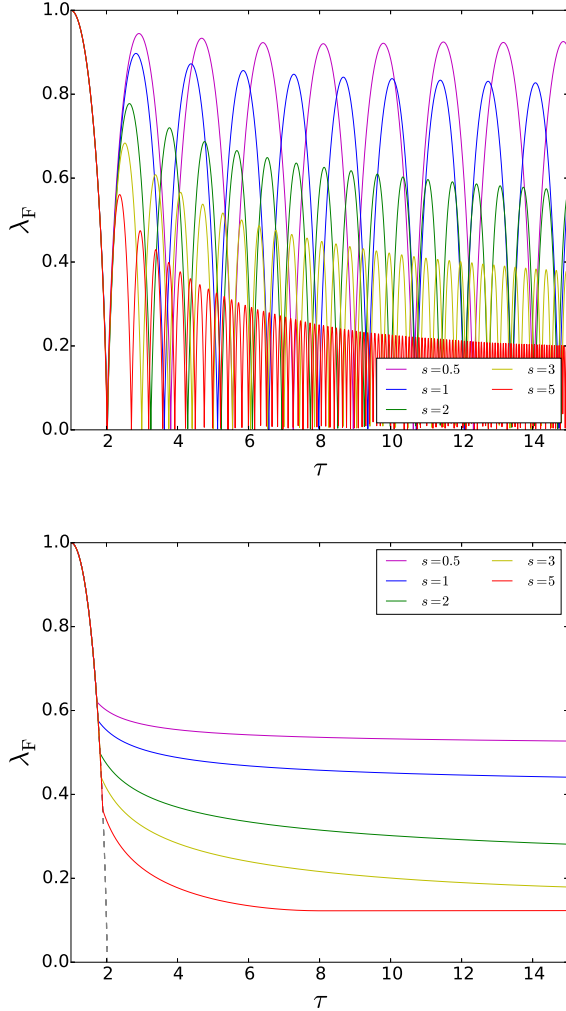


Figure 3. Another view of the trajectories of self-similar infall of dark matter (upper panel) and gas (lower panel). Same as Fig. 2 but with the radii of the accreted shells normalized to their turn-around radius, i.e. $\lambda_F = r/r^*$, and the time normalized to their turn-around time, i.e. $\tau = t/t^*$. The gray dashed line in the lower panel shows the trajectory for the dark matter for a comparison.

locations. Expressed in a dimensionless form, it is

$$\frac{1}{2} \left(\frac{d\lambda_F}{d\tau} \right)_{\text{sh}}^2 = \frac{2M_{\text{ta}}}{9} \left(\frac{1}{\lambda_{F,\text{sh}}} - 1 \right), \quad (8)$$

or in terms of the dimensionless pre-shock velocity V_1 (see Ta-

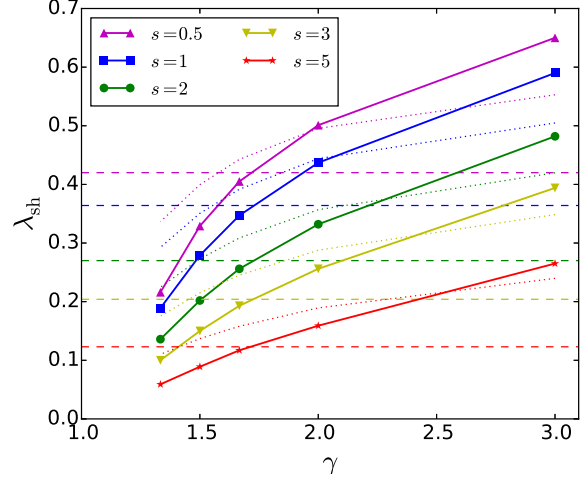


Figure 4. Positions of the accretion shock for gas with various adiabatic indices γ , and for various accretion rates s indicated by the color. The splashback positions of the collisionless matter are marked by the dashed lines. The dotted lines show the approximate estimation of the shock position using Eqs. (9) and (10).

ble 1),

$$\frac{1}{2} V_1^2 \tau_{\text{sh}}^{2\delta-2} = \frac{2M_{\text{ta}}}{9} \left(\frac{1}{\lambda_{\text{sh}} \tau_{\text{sh}}^\delta} - 1 \right). \quad (9)$$

Here we have taken the mass enclosed in the infalling shell to be a constant, which holds unless accretion shock happens significantly inside the splashback radius of the dark matter.

The properties of the post-shock halo gas are harder to approximate to a good precision with a simple analytical form. For a very crude estimation, we take the approximation $V_2 \approx 0$ which would mean that the post-shock gas is at perfect hydrostatic equilibrium. This approximation suggests (from the first equation in the shock jump conditions Eq. 7)

$$(V_1 - \delta \lambda_{\text{sh}}) \frac{\gamma - 1}{\gamma + 1} + \delta \lambda_{\text{sh}} \approx 0. \quad (10)$$

In the actual solutions, some residue gas motion still exists after the accretion shock (see the upper middle panel of Fig. 1).

Now, combining Eqs. (9) and (10) allows us to derive an approximation for the accretion shock location λ_{sh} . Despite the approximations, the result gives the correct trends of how λ_{sh} depends on the control parameters δ and γ (see the dotted lines in Fig. 4)², confirming that the accretion shock position is determined

² For the estimation, we fix $\tau_{\text{sh}} = 2$ which is a rough approximation based on the symmetry of expansion and infall around the turn-around point (by

from the continuities of the halo gas which is approximately in hydrostatic equilibrium and the pre-shock gas which carries kinetic energy gained during the gravitational infall. It also helps us to understand the parameter dependencies (Fig. 4 and Table. 2): both a smaller adiabatic index γ and a larger accretion rate s require a larger pre-shock velocity V_1 at a certain shock position λ_{sh} to satisfy the shock jump conditions Eq. (10), which implies a smaller λ_{sh} since it allows more conversion of the gravitational energy (Eq. 9) and thus gives a higher pre-shock velocity.

3.2 Comparison with the dark matter splashback radius

State-of-the-art hydrodynamical numerical simulations have found the curious result that the accretion shock radius of the gas and the splashback radius of the dark matter follow each other closely (Lau et al. 2015) despite the very different physical processes involved. Is this a pure coincidence or is there some physical reason behind?

It was already noticed by Bertschinger (1985) that this result holds true only for a gas with an adiabatic index $\gamma \approx 5/3$, for an accretion rate he studied. We extend his analysis to an arbitrary value of the accretion rate. In Fig. 4, we show the positions of the splashback radius with the horizontal dashed lines. We find that, for and only for $\gamma \approx 5/3$, the accretion shock position aligns well with the splashback radius for all the tested accretion rates. The mystery is then two-folds: why for $\gamma \approx 5/3$, and more intriguingly, why does this alignment hold at $\gamma \approx 5/3$ for any accretion rate?

To find the answers we now consider the origin of the splashback radius of the dark matter. Initially, the dark matter shares the same expansion and infall with the gas and obeys Eq. (8). It then enters the multi-stream region when it reaches λ_{sp} , and starts to oscillate around the cluster center in the potential well of the cluster. The approximate position of the splashback radius can be given analytically by considering this process, yielding (Shi 2016)

$$\lambda_{\text{sp}} \approx \begin{cases} 3^{-\delta} & \text{if } \delta \leq 1 \ (s \leq 3/2), \\ \left[1 + 4(2\delta - 1)/\sqrt{\pi}\right]^{-1} & \text{if } \delta \geq 1 \ (s \geq 3/2). \end{cases} \quad (11)$$

Once again, $\delta = 2(1 + s/3)/3$. The two regimes of accretion $\delta \leq 1$ and $\delta > 1$ correspond to an approximately constant inner gravitational potential well and one growing with time, respectively. Due to the increase of the turn-around radius r_{ta} with time, the amplitude of the oscillation in terms of λ decreases with time (Fig. 2) even when $\delta \leq 1$, and thus $\lambda_{\text{sp}} < 1$ for all non-vanishing mass accretion rates.

The alignment of the two radii holds for an adiabatic gas with $\gamma \approx 5/3$ for $0.5 \leq s \leq 5$ suggests that for this range of mass accretion rates, the dynamical effect of the accretion shock on a $\gamma \approx 5/3$ gas mimicks that of the growth of the cluster and r_{ta} on the dark matter. The value $\gamma \approx 5/3$ reflects nothing more fundamental, and may not apply for more extreme mass accretion rates either. In fact, combining the approximate expressions for λ_{sh} (Sect. 3.1) and λ_{sp} (Eq. 11) suggests that for higher mass accretion rates $s > 6$, harder adiabatic indices ($\gamma > 5/3$) are required for the accretion shock position to align with the splashback radius.

Both the accretion shock and the splashback radius decrease with a higher mass accretion rate but for different reasons. For the gas, it is because a higher mass accretion rate s suggests higher

definition, $\tau = 1$ at turn-around). The precise value of τ_{sh} is slightly smaller than 2 and varies with the accretion rate and the adiabatic index of the gas (see Fig. 3)

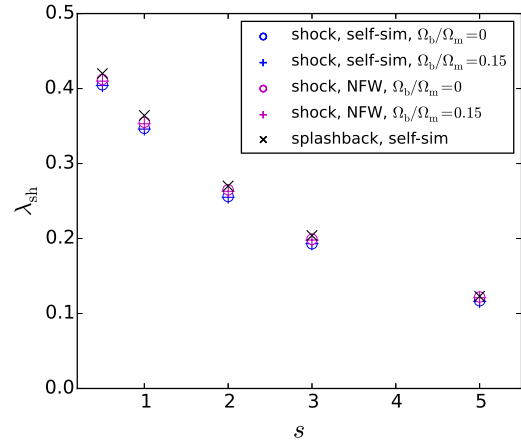


Figure 5. Positions of the accretion shock of an adiabatic gas with $\gamma = 5/3$ compared to the splashback position of dark matter (black crosses) for various accretion rates s . The shock radius is computed with various total mass profiles, including a self-similar profile (blue markers) and that with inner profile modified to an NFW shape (magenta markers), both with $\Omega_b/\Omega_m = 0$ ('o') or $\Omega_b/\Omega_m = 0.15$ ('+').

energy and momentum of the inflowing gas, whereas for the dark matter, it is due to a more significant cluster growth during the time between the splashback and when the matter at splashback was accreted. That their dependencies on the mass accretion rate are so similar for the range of accretion rates we tested is likely just a coincidence.

3.3 Effect of relaxation and Ω_b

How representative is the accretion shock radius from the $\Omega_b = 0$ self-similar solution that has a power-law inner mass profile? Here we explore the influence of a finite baryon content $\Omega_b/\Omega_m = 0.15$ close to the observed values (Komatsu et al. 2011; Planck Collaboration XIII 2015) and a more realistic NFW mass profile (Navarro, Frenk & White 1996, 1997) on the accretion shock position. Both the two modifications should influence the accretion shock position through their change to the total mass profile. Since the self-similar solutions of the gas and dark matter mass profiles in the $\Omega_b = 0$ case are very similar for a $\gamma = 5/3$ gas (Fig. 1), the change to the total mass profile by a moderate baryon content is expected to be small, and thus a direct modification of the shape of the inner mass profile to an NFW profile is expected to give a greater change to the accretion shock position.

The way we embed an NFW profile in the inner region of the halo follows that of Adhikari, Dalal & Chamberlain (2014). We determine the concentration parameter c by requesting that the slope of the NFW profile at the virial radius is equal to the inner mass slope Υ of the self-similar solution, i.e. $c^2/(1 + c)^2/m_{\text{nfw}}(c) = \Upsilon$ with $m_{\text{nfw}}(x) = \ln(1 + x) - x/(1 + x)$, and the asymptotic inner dark matter mass slope as derived by Fillmore & Goldreich (1984)

$$\Upsilon = \begin{cases} 3s/(s + 3) & \text{if } s \leq 3/2 \\ 1 & \text{if } s \geq 3/2. \end{cases} \quad (12)$$

The results confirm our expectations on the changes to the accretion shock radius (Fig. 5 and Table. 3), and also shows that even modifying the inner total mass profile from the self-similar solution to an NFW profile only slightly increases the shock radius.

Table 3. Tabular form of Fig. 5. Positions of the accretion shock (columns 2-5), λ_{sh} , compared to the splashback position of the collisionless matter (columns 6), λ_{sp} , for various accretion rate s .

	Self-similar, $\Omega_b/\Omega_m = 0$	Self-similar, $\Omega_b/\Omega_m = 0.15$	NFW, $\Omega_b/\Omega_m = 0$	NFW, $\Omega_b/\Omega_m = 0.15$	Self-similar, splashback
$s = 0.5$	0.405	0.404	0.412	0.410	0.420
$s = 1$	0.347	0.346	0.355	0.353	0.364
$s = 2$	0.256	0.255	0.265	0.263	0.270
$s = 3$	0.193	0.193	0.199	0.198	0.204
$s = 5$	0.117	0.116	0.122	0.121	0.123

For a first-order estimation, the effect of relaxation and a moderate nonzero baryon content on the accretion shock position can be neglected³.

4 ICM PROPERTIES

Analytical models based on a smooth accretion picture have been successful in explaining some basic observed properties of the ICM, in particular its entropy profile (Tozzi & Norman 2001; Voit et al. 2003), despite the cluster growth being partly clumpy rather than smooth. Here we show that, even with the self-similar spherical collapse model which perhaps can be considered as the simplest smooth accretion model, some of the observed ICM properties are already captured, and insights on their underlying physics can be obtained.

Since the gas is considered as adiabatic after the accretion shock in the self-similar spherical collapse model, the effects of radiative cooling and feedback processes are absent in our results. This needs to be kept in mind when interpreting the ICM properties especially in the cluster core region where these effects are significant.

4.1 Gas mass profile

The M_{gas} profile in the self-similar solution is close to a power-law inside the accretion shock (Fig. 1). This guarantees that the gas density, entropy, and pressure profiles are also approximately of power-law shape (see the next subsection). For a small accretion rate $s \leq 3/2$, the power-law slope α_M of M_{gas} is almost identical to that of M_{dm} , because the both the trajectory of a shell of gas and the apoapsis of the dark matter trajectory approach a finite Eulerian radius (Fig. 3). For a larger accretion rate, the trajectory of a gas shell still stops at a finite radius, but the orbit of a dark matter shell continues to shrink in amplitude, and thus leads to a shallower mass slope than that of the gas.

The above physical picture motivates us to find an approximation for α_M based on the asymptotic mass slope for the dark matter Υ , which takes account of the additional steepening of gas mass slope compared to that of the dark matter at large accretion rates,

$$\alpha_M \approx \begin{cases} 3s/(s+3) & \text{if } s \leq 3/2 \\ 9(s+1)/(s+3)/5 & \text{if } s \geq 3/2. \end{cases} \quad (13)$$

The slope α_M monotonously steepens with accretion rate s , and ranges from 0.8 for $s = 0.5$ to 1.4 for $s = 5$ (Fig. 6). For a mass

³ On the other hand, the effect of inner mass profile on the splashback radius is larger at high mass accretion rates, as suggested by the dependence of the r_{sp} value on the concentration parameter of NFW-shape halos (Shi 2016).

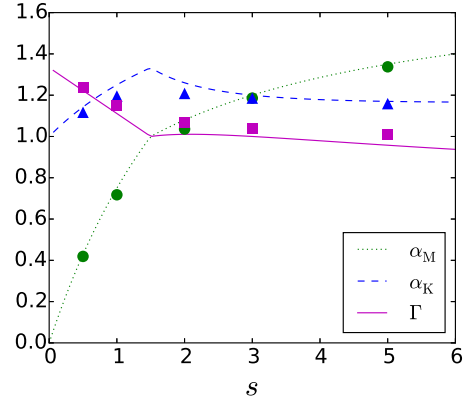


Figure 6. Logarithmic slope for the gas mass profile (green), entropy profile (blue), and the effective polytropic index Γ (magenta) as functions of the accretion rate s . The markers show values fitted using the self-similar solution on the radial range $0.01\lambda_{\text{sh}} < \lambda < 0.5\lambda_{\text{sh}}$. The lines show the analytical estimations given by Eqs. (13), (15) and (16).

accretion rate $s > 3/2$, the mass slope depends also on the adiabatic index of the gas, and the expression above is valid only for $\gamma = 5/3$ (see Appendix. B).

4.2 Entropy profile

Being constant in adiabatic processes, entropy records the heating and cooling history of the ICM. Thus the entropy profile is a very useful physical property that describes the structure of the ICM.

The key idea of the smooth accretion models is that the entropy distribution in the ICM is primarily set by the cluster's mass accretion history, i.e. the entropy and the mass of the gas are correlated. Since the post-shock flow is adiabatic, the entropy of the gas is set at the accretion shock in a smooth accretion model. The intracluster gas entropy can thus be used as a Lagrangian variable like the gas mass M_{gas} , and therefore a simple relation between the two is expected.

Combining the mass and entropy integrals (Appendices. A1 and A2) we find this relation to be (cf. Bertschinger 1983)

$$K \propto M_{\text{gas}}^{-\zeta} \quad (14)$$

in the self-similar model, with $-\zeta = 2(\gamma + \delta - 2)/(3\delta - 2) = (2s + 3)/(s + 3)$ varying from 2.7 for $s = 0.5$ to 0.9 for $s = 5$. Note that this relation is derived simply from the continuity and the adiabatic equations, without making use of the shock jump conditions which is the basis of the $K(M, \dot{M})$ relation in the other smooth accretion models (Tozzi & Norman 2001; Voit et al. 2003).

Considering that the mass accretion rate may change (even

significantly) throughout the assembly of a galaxy cluster, a more generalized version of this relation is $d \ln K / d \ln r = -\zeta (d \ln M_{\text{gas}} / d \ln r)$, that the local logarithmic slopes of the entropy and gas mass profiles are linearly related with a pre-factor depending on the accretion rate. Since both the entropy and the gas mass can be inferred directly from X-ray and millimetre observations of galaxy clusters, it would be interesting to test this generalised relation in observations and numerical simulations to see to which degree it holds in a more realistic mass accretion scenario as well as when secondary effects such as cooling and additional ways of entropy injection e.g. AGN feedback are present. In case the relation holds well in more realistic conditions, testing how the relation between entropy and gas mass slopes depends on the mass accretion rate in simulations may potentially lead to a method of inferring the mass accretion history.

With Eqs. (13) and (14) we can estimate the logarithmic slope of the entropy profile as

$$\alpha_K = -\zeta \alpha_M. \quad (15)$$

Remarkably, although both ζ and the gas mass slope α_M vary quite significantly with the accretion rate, the value of the entropy slope stays within a small range $\alpha_K \sim 1.1 - 1.2$ (Fig. 6). The inferred values of the entropy slope also match with that of the ‘baseline intracluster entropy profile’ (Voit, Kay & Bryan 2005), which presents the theoretical expectation from a smooth accretion model as well as from adiabatic hydrodynamical simulations. Many observed entropy profiles do follow a power-law shape with a similar slope between the cluster core regions where they are significantly modified by cooling and feedback processes, and the cluster outskirts where the measurement becomes much harder and still controversial (e.g. Walker et al. 2012; Eckert et al. 2013, and referenced therein).

4.3 Effective equation of state

Analytical models of the ICM profiles often make the approximation that the intracluster gas has an effective equation of state $p \propto \rho^\Gamma$ where the value of Γ does not depend on radius (Lea 1975; Komatsu & Seljak 2001; Shaw et al. 2010). This is found by hydrodynamical numerical simulations to be precise to $\sim 10\%$ in the virial regions of galaxy clusters (e.g. Shaw et al. 2010; Battaglia et al. 2012), and the value for this effective polytropic index $\Gamma \sim 1.1 - 1.2$ matches the observations (e.g. Eckert et al. 2013).

For the self-similar solutions, the approximate effective polytropic index can be estimated given α_K and the logarithmic slope of the density profile $\alpha_D = \alpha_M - 3$, as

$$\Gamma = \alpha_K / \alpha_D + \gamma = \gamma - \zeta \alpha_M / (\alpha_M - 3). \quad (16)$$

Like α_K , the approximate values for Γ also stay within a small range when the accretion rate varies (Fig. 6). In detail, Γ slightly decreases at larger accretion rates. This is in agreement with the weak positive correlation between Γ and the concentration parameter of the dark matter halo found in Komatsu & Seljak (2001, 2002)⁴.

This effective polytropic index Γ differs physically from the

⁴ In fact, using the method described in Sect. 3.3 to match the accretion rate and the concentration parameter, our accretion rate dependence of Γ agrees with the Komatsu & Seljak (2002) fitting formula (their equation 17) both in their trends and also quantitatively to $< 5\%$ for $0.5 \leq s \leq 5$. Although we cannot rule out the possibility of this being a coincidence, this makes it more interesting to look for this weak but monotonous dependence of Γ on the accretion rate or on the concentration parameter in hydrodynamical simulations and observations.

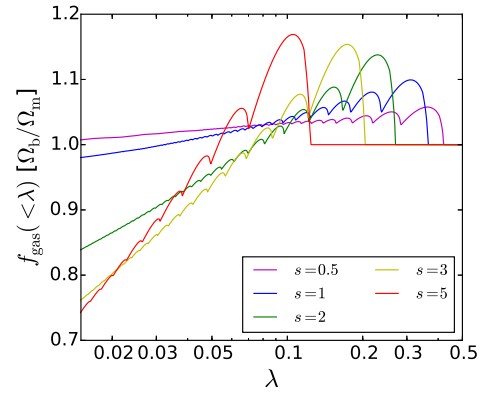


Figure 7. Gas mass fraction of the self-similar solutions for various accretion rates (lines with different colors). The values are normalised to the cosmic mean gas mass fraction Ω_b/Ω_m .

polytropic index, or the adiabatic index of the gas γ . While the latter reflects how the gas pressure changes under compression or expansion, the former is merely an effective description of the global ICM structure. Nevertheless, one may wonder why the ICM structure is characterised by an effective polytropic index $\Gamma < \gamma$. From the relation Eq. (16) above, the value of Γ is set by the $K(M_{\text{gas}})$ relation which describes the entropy generation during mass accretion, and the gas mass profile itself⁵. That $\Gamma < \gamma$ is simply due to a positive slope of the entropy profile α_K as a result of an increasing entropy production at the accretion shock with growing mass of the cluster.

4.4 Gas mass fraction

In observations, the gas mass fraction $f_{\text{gas}} = M_{\text{gas}}/M$ is typically found to be less than the cosmic mean value at small radii, and approaches the cosmic mean around the virial radius of the cluster (e.g. Pratt et al. 2010; Eckert et al. 2013). This has been commonly regarded as evidence for feedback by e.g. AGNs in the central galaxies which expels the inner baryonic material to large radii and even out of the potential well of the halo. Such an interpretation is supported by the observation of progressively more significant baryon loss from clusters of galaxies, groups of galaxies to galaxies themselves (e.g. Dai et al. 2010, and references therein).

Here we consider an additional cause to the deviation of the gas mass fraction from the cosmic mean value: that gas lagging behind dark matter during its infall on to the cluster after going through the accretion shock. Fig. 7 shows the gas mass fraction in the self-similar solutions as influenced by the accretion shock. Unlike the entropy profile and the effective equation of state of the ICM, we find the gas mass fraction to depend strongly on the mass accretion rate. The higher the mass accretion rate, the stronger the depletion of gas relative to the dark matter in the inner regions of the cluster. The depletion is already more than 20% at $0.1 r_{\text{sh}}$ for a mass accretion rate $s \geq 3$. This is again caused by the stronger adiabatic contraction at high accretion rates, which steepens the gravitational potential in the central regions and causes the orbits of the dark matter to contract further in comparison with the gas. Since the effect of this accretion dynamics on the f_{gas} is most likely

⁵ This is also noticed in Voit et al. (2003). However, a Γ value of $\sim 1.1 - 1.2$ does not require a near linear relation between K and M_{gas} as stated there.

secondary to that of the AGN feedback, the f_{gas} profiles presented here may not be realistic. Nevertheless, the strong dependence of the inner gas fraction on the mass accretion rate found here may be observable, which encourages one to study this dependence in numerical simulations and in observations.

5 DISCUSSIONS

5.1 Effect of deviation from smooth accretion

In the hierarchical structure formation picture, galaxy clusters grow not all via smooth accretion as assumed in this paper and by other smooth accretion models. Mergers and accretion through filaments are also significant modes of accretion. They destroy the Lagrangian nature of the radial coordinate by mixing matter accreted at different times, and they introduce density inhomogeneities to the ICM. Quantitative effects of these are hard to evaluate and remain an open question.

Voit et al. (2003) addressed the effect of density inhomogeneities in the material being accreted on the entropy of the ICM. They find that a homogeneous accretion maximizes the observed entropy as a pure effect of mass-weighting during the averaging. Similarly, mass-weighted accretion shock radius would be biased towards that of the higher density gas. As gas with slightly higher density carries more momentum per volume, it would get shocked at a smaller radius, and thus density inhomogeneities would lead to a smaller mass-weighted accretion shock radius.

Mixing of matter accreted at different times tends to wash out the dependence of the ICM profiles on the mass accretion history. Supposedly, it would at the same time drive the profiles towards a more ‘relaxed’ state. However, since the ICM structure given by smooth accretion models with a typical mass accretion history is generally already stable and smooth, the effect of this radial mixing may not be prominent in reality.

5.2 Effect of Dark Energy

Throughout the paper we have been studying the accretion shock location and the ICM profiles in an Einstein de-Sitter universe where self-similarity strictly holds. How would our results change in a Λ CDM universe with a non-zero dark energy content?

The effect of dark energy is mainly on the dynamics of dark matter and gas before they turn around. Within the turn-around radius, the gravity of the halo dominates and the role of dark energy is negligible. In this sense, the effect of dark energy on the properties of the cluster region is through the initial condition at turn-around, and can partly be mimicked by a change of the mass accretion rate s . Thus, we expect the features that have little dependence on s to remain in a Λ CDM universe, such as that the logarithmic slope of entropy profile and the effective polytropic index of the intracluster gas lying in a narrow range of 1.1–1.2, and that the shock radius aligns well with the dark matter splashback radius for moderate accretion rates $s \lesssim 5$. The latter, combined with the origin of the good scaling between splashback radius and $r_{200\text{m}}$ (Shi 2016), would also suggest that the accretion shock scales well with $r_{200\text{m}}$ for a similar reason: the correlated increase of the matter content of the universe and the average halo mass accretion rate with redshift, and their canceling effects on $r_{\text{sh}}/r_{200\text{m}}$.

Quantitative estimations of the effect of dark energy requires an extension of the current framework to a Λ CDM universe, where

the evolution of the cosmological background introduces an additional time scale to the system and breaks the strict self-similarity. In this case, we can consider the change of the cosmological background as described by e.g. the matter content Ω_m as an adiabatic variable, and approximate the relatively fast dynamics of gas and dark matter as self-similar for each Ω_m value. The extension for the dark matter has already been achieved in Shi (2016) and have yielded results confirming our expectations. We leave the extension for the gas to future work.

6 CONCLUSION

Although simple and fully analytical, the self-similar spherical collapse model already captures some fundamental ICM properties such as the location of the accretion shock, its alignment with the splashback radius, the entropy profile and the effective polytropic index of the intracluster gas. We have systematically studied the ICM properties given by the self-similar spherical collapse model for dark matter and gas by extending Bertschinger’s work to various mass accretion rates. We also consider the effect of a different inner mass profile due to dynamical relaxation, and the effect of a moderate baryon content.

Our main findings can be summarised as follows.

- The radial position of the accretion shock is set by the continuities of mass, momentum and enthalpy between the approximately hydrostatic cluster gas and the gas being accreted by the cluster. Neither a modification of the inner mass profile to an NFW shape due to dynamical relaxation nor the exact value of the baryon content has much effect on the accretion shock location.
- The alignment of the accretion shock radius and splashback radius discovered in hydrodynamical simulations is *not* universal, in the sense that it holds only for a gas with an adiabatic index of $\gamma \approx 5/3$ and for not-too-high mass accretion rates. For the intergalactic gas for which $\gamma \approx 5/3$, the alignment indeed holds for a large range of low and moderate accretion rates $s \lesssim 5$ which are typical for galaxy clusters at low redshifts. This arises from the dependencies of the accretion shock and the splashback radius on the accretion rate, which are the same in direction and similar in degree, but different in physics. For the gas, it is because the higher energy and momentum of the inflowing gas associated with a higher mass accretion rate. For the dark matter, it is due to a more significant halo growth during the time between the splashback and when the matter at splashback was accreted.
- In the self-similar spherical collapse model, like in any smooth accretion model, the entropy distribution in the ICM is set by the cluster’s mass accretion history. However, the logarithmic slope of the entropy profile is rather independent of the mass accretion rate and lies around 1.1 – 1.2. This confirms the robustness of the ‘baseline intracluster entropy profile’ of Voit, Kay & Bryan (2005).
- A linear relation exists between the local logarithmic slopes of the entropy and gas mass profiles, with a pre-factor depending on the mass accretion rate. Although based on a heavily simplified picture, this relation is worth testing in hydrodynamical simulations and observations, and may lead to a method of constraining the mass accretion history of galaxy clusters from observations of the ICM.
- This effective polytropic index of the intracluster gas is an effective description of the global ICM structure, and is set by the gas mass profile and the entropy generation during mass accretion. It also has a value around 1.1 – 1.2 and is rather independent of the

mass accretion rate. Its value is smaller than that of the actual polytropic index (the adiabatic index) of the gas as a result of the cluster mass growth and the consequent increasing entropy production at the accretion shock.

- The accretion shock slows down the gas compared to the dark matter during their accretion on to a galaxy cluster, and leads to a deficit of gas mass fraction compared to the cosmic mean in the inner regions of the cluster. Unlike the entropy profile and the effective polytropic index of the ICM, this effect depends strongly on the mass accretion rate of the cluster. This calls for simulation and observation studies of f_{gas} as a function of the mass accretion rate.

ACKNOWLEDGEMENTS

XS is grateful to Eiichiro Komatsu for carefully reading the manuscript and giving helpful suggestions, as well as to Erwin Lau for discussions and comments, and to Daisuke Nagai for related discussions during his visit at MPA.

REFERENCES

- Adhikari S., Dalal N., Chamberlain R. T., 2014, JCAP, 11, 19
 Battaglia N., Bond J. R., Pfrommer C., Sievers J. L., 2012, ApJ, 758, 75
 Bertschinger E., 1983, ApJ, 268, 17
 Bertschinger E., 1985, ApJS, 58, 39
 Dai X., Bregman J. N., Kochanek C. S., Rasia E., 2010, ApJ, 719, 119
 Diemer B., Kravtsov A. V., 2014, ApJ, 789, 1
 Eckert D., Ettori S., Molendi S., Vazza F., Paltani S., 2013, A&A, 551, A23
 Fillmore J. A., Goldreich P., 1984, ApJ, 281, 1
 Kang H., Ryu D., Cen R., Ostriker J. P., 2007, ApJ, 669, 729
 Komatsu E., Seljak U., 2001, MNRAS, 327, 1353
 Komatsu E., Seljak U., 2002, MNRAS, 336, 1256
 Komatsu E. et al., 2011, ApJS, 192, 18
 Lacey C., Cole S., 1993, MNRAS, 262, 627
 Lau E. T., Nagai D., Avestruz C., Nelson K., Vikhlinin A., 2015, ApJ, 806, 68
 Lea S. M., 1975, Astrophys. Lett., 16, 141
 More S., Diemer B., Kravtsov A. V., 2015, ApJ, 810, 36
 Navarro J. F., Frenk C. S., White S. D. M., 1996, ApJ, 462, 563
 Navarro J. F., Frenk C. S., White S. D. M., 1997, ApJ, 490, 493
 Planck Collaboration XIII., 2015, preprint (arXiv: 1502.01589)
 Planck Collaboration XL., 2015, preprint (arXiv: 1511.05156)
 Planelles S., Quilis V., 2013, MNRAS, 428, 1643
 Pratt G. W. et al., 2010, A&A, 511, A85
 Reiprich T. H., Basu K., Ettori S., Israel H., Lovisari L., Molendi S., Pointecouteau E., Roncarelli M., 2013, Space Sci. Rev., 177, 195
 Shaw L. D., Nagai D., Bhattacharya S., Lau E. T., 2010, ApJ, 725, 1452
 Shi X., 2016, MNRAS, 459, 3711
 Tozzi P., Norman C., 2001, ApJ, 546, 63
 Vazza F., Dolag K., Ryu D., Brunetti G., Gheller C., Kang H., Pfrommer C., 2011, MNRAS, 418, 960
 Voit G. M., Balogh M. L., Bower R. G., Lacey C. G., Bryan G. L., 2003, ApJ, 593, 272
 Voit G. M., Kay S. T., Bryan G. L., 2005, MNRAS, 364, 909

Walker S. A., Fabian A. C., Sanders J. S., George M. R., 2012, MNRAS, 427, L45

APPENDIX A: INTEGRALS OF MOTION

Bertschinger (1985) has identified three integrals of motion for the self-similar spherical collapse solution of dark matter and gas with $\Omega_b \ll 1$. Apart from providing checks for the numerical solution, we find them valuable for understanding the shapes of the ICM profiles (Sect. 4). Here we derive these integrals of motion for an arbitrary accretion rate s .

A1 Mass integral

To keep self-similarity, the fraction of gas mass within a radius λ should stay constant with time. This gives a relation between the gas mass and its flux (cf. Bertschinger 1983),

$$\frac{m_{\text{gas}}}{m_{\text{gas,ta}}} = \frac{4\pi r_{\text{ta}}^2 \rho(\lambda v_{\text{ta}} - v)}{4\pi r_{\text{ta}}^2 \rho_{\text{ta}} v_{\text{ta}}}. \quad (\text{A1})$$

Using Eq. (2), and that

$$\rho_{\text{ta}} = \frac{m_{\text{gas,ta}}}{4\pi r_{\text{ta}}^3} \frac{d \ln m_{\text{ta}}}{d \ln t} \left(\frac{d \ln r_{\text{ta}}}{d \ln t} \right)^{-1} = \frac{m_{\text{gas,ta}}}{4\pi r_{\text{ta}}^3} \frac{2s}{3\delta} \quad (\text{A2})$$

to express Eq. (A1) in terms of the nondimensional quantities, it is

$$M_{\text{gas}} = -\frac{9}{2s} \lambda^2 D \bar{V}, \quad (\text{A3})$$

with $\bar{V} = V - \delta \lambda_{\text{sh}}$ being the velocity in the frame where the shock is static.

A2 Entropy integral

We re-write the continuity and adiabatic equations of the gas (the first and the third equations of the fluid equations Eq. 6) as

$$\begin{aligned} (\ln \lambda^2 D \bar{V})' &= -\frac{3\delta - 2}{\bar{V}}, \\ (\ln K)' &= (\ln P)' - \gamma (\ln D)' = -\frac{2(\gamma + \delta - 2)}{\bar{V}}. \end{aligned} \quad (\text{A4})$$

In this form, it is straightforward to derive that $K(\lambda^2 D \bar{V})^\zeta = \text{const}$, with

$$\zeta = -\frac{2(\gamma + \delta - 2)}{3\delta - 2} = -\frac{2}{3} - \frac{1}{s}. \quad (\text{A5})$$

A3 Virial theorem

The two integrals of motion above are local ones which is valid at each radius. Another global integral of motion is provided by the virial theorem. The dimensionless specific kinetic, thermal and gravitational energies averaged within the accretion shock are (Bertschinger 1985)

$$\begin{aligned} t &= \int_0^{M_2} \frac{V^2}{2} dM \\ u &= \int_0^{M_2} \frac{P/D}{\gamma - 1} dM \\ w &= -\frac{2}{9} \int_0^{M_2} \frac{M_x}{\lambda} dM. \end{aligned} \quad (\text{A6})$$

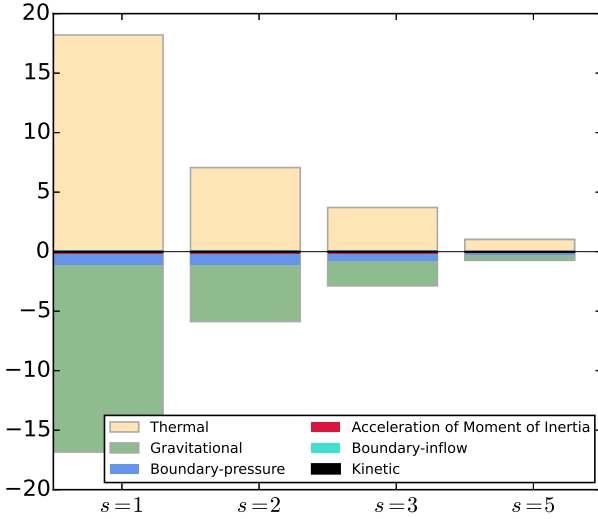


Figure A1. Test of the virial theorem in the shock-enclosed region. Kinetic, thermal, gravitational energy terms of Eq. (A7) are shown, as well as the acceleration of the moment of inertia, and the boundary terms from mass inflow and gas pressure. The $s = 0.5$ case is not shown because there the thermal and gravitational energies diverge at $r = 0$.

The virial theorem can be derived from the Euler equation in Eq. (6) as

$$\begin{aligned} & \left(\frac{25}{2} \delta^2 - \frac{25}{2} \delta + 3 \right) \int \lambda^2 dM \\ &= 2t + 3(\gamma - 1)u + w \\ & - 3\lambda_s^3 D_2 \bar{V}_2 \left[\bar{V}_2 + \frac{7\delta - 3}{2} \lambda_s \right] - \frac{6}{\gamma - 1} \lambda_s^3 D_2 \bar{V}_2^2. \end{aligned} \quad (\text{A7})$$

The l.h.s. is $d^2 I / dt^2$ where I is the moment of inertia. The two boundary terms on the r.h.s. can be interpreted as originating from the flux of inertia through the boundary and the pressure at the boundary respectively⁶. The second boundary term $-6\lambda_s^3 D_2 \bar{V}_2^2 / (\gamma - 1)$ can be also expressed as $-3P_2 \lambda_s^3$.

With the numerical self-similar solution presented in this paper, the sum of all terms is approximately zero with a deviation less than one percent of the thermal energy. As shown in Fig. A1, the thermal and gravitational energy are the dominating terms in the virial theorem. The other terms are (in decreasing order of their magnitudes): the second boundary term, the acceleration of the moment of inertia, the first boundary term, and the kinetic energy.

APPENDIX B: INFLUENCE OF THE ADIABATIC INDEX ON THE ICM PROFILES

The diffuse intergalactic gas that accretes on to galaxy clusters is composed dominantly of ionized single-atom particles, and thus has an adiabatic index $\gamma = 5/3$. Nevertheless, exploring how the ICM properties depend on the adiabatic index can lead to a better understanding of the physical origin of the ICM profiles. Also, as a means of entropy reduction, the effect of radiative cooling can be

mimicked by a softer (smaller) adiabatic index; as an additional entropy injection mechanism, AGN feedback can be mimicked by a stiffer (larger) adiabatic index. Thus studying cases for gas with different adiabatic indices also allows one to see roughly what effects cooling and AGN feedback have on the ICM profiles.

Figs. B1 and B2 present the self-similar ICM profiles for gas with various adiabatic indices ranging from $\gamma = 4/3$ that corresponds to a gas with six degrees of freedom e.g. a diatomic gas at high temperature, to $\gamma = 3$ that corresponds to a gas with only one degree of freedom. Except for the change on the accretion shock location that has been discussed in Sect. 3, the most prominent effect of γ on the ICM is a steeper entropy profile at a stiffer adiabatic index, which is reflected in the adiabatic equation e.g. the second equation in Eq. (A4). Another influence of different γ values is prominent only at high accretion rate: the gas mass profile also steepens with a stiffer adiabatic index when $s > 3/2$. The gas density and pressure profile slopes, the effective polytropic index, and the gas mass fraction are also affected as a consequence (see Sect. 4).

⁶ The second boundary term is missing in the virial theorem expression in Bertschinger (1985). It is larger than the first boundary term in magnitude (Fig. A1).

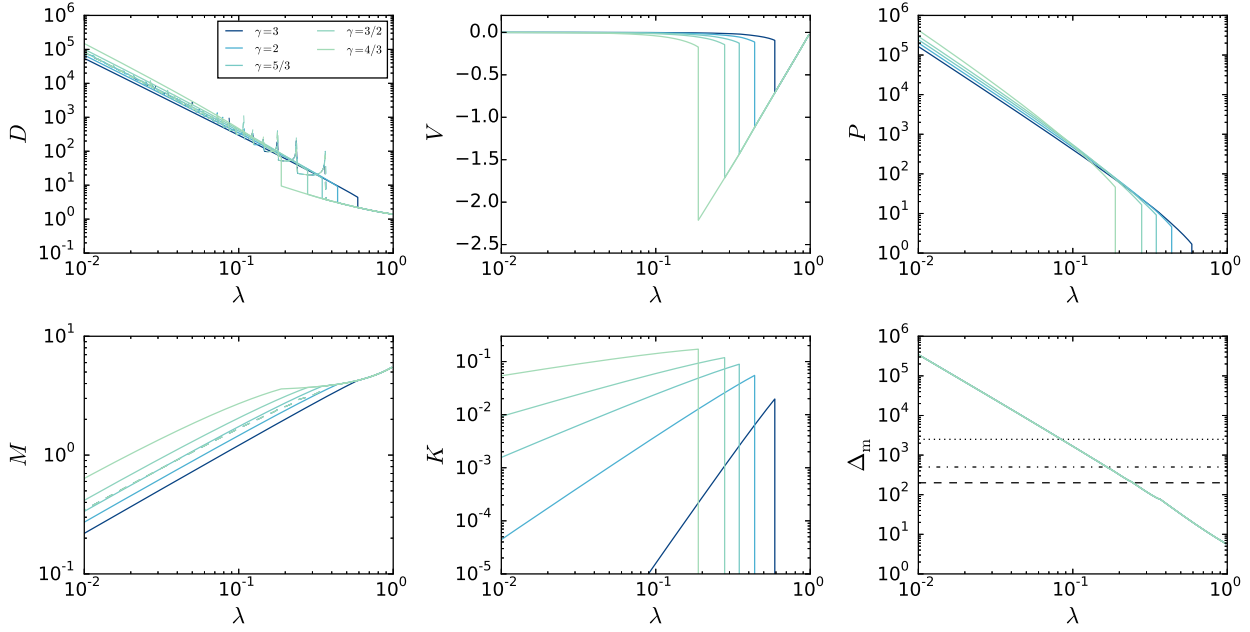


Figure B1. Dimensionless ICM profiles of the self-similar spherical collapse model. Similar to Fig. 1 but showing the dependency of the profiles on the adiabatic index γ of the gas. A mass accretion rate of $s = 1$ is used.

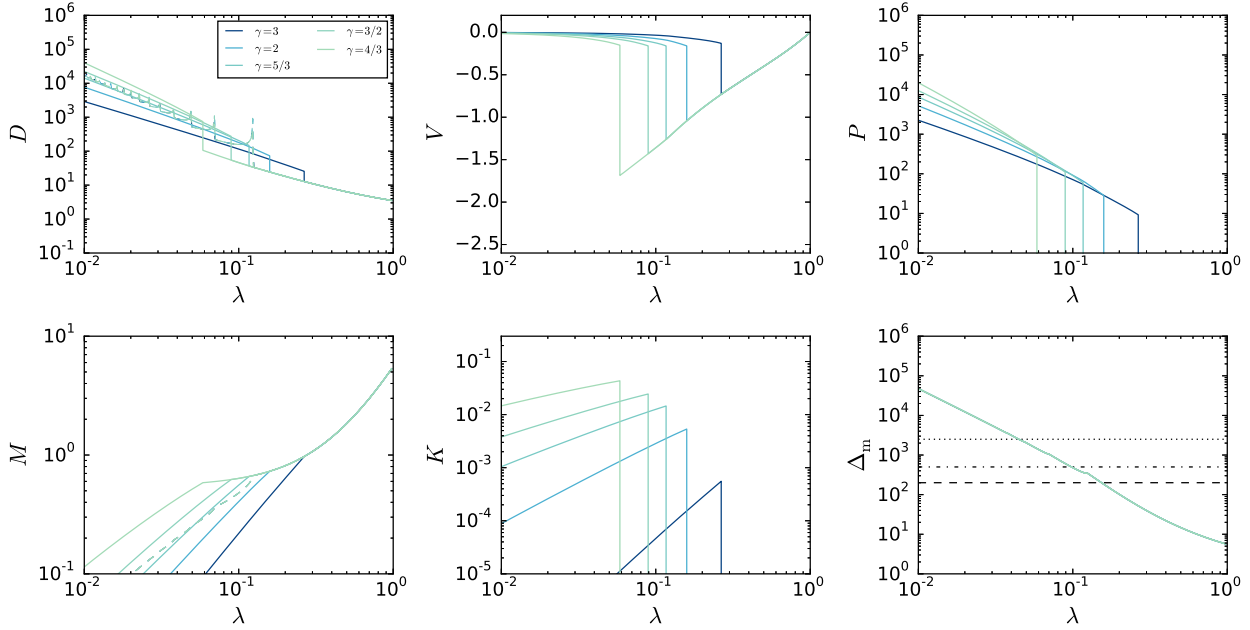


Figure B2. Same as Fig. B1 but for a mass accretion rate of $s = 5$.